Journal of Sol-Gel Science and Technology 38, 13–17, 2006

DOI: 10.1007/s10971-005-5630-5

Sol-gel Preparation of Fluoridated Hydroxyapatite in $Ca(NO_3)_2$-$PO(OH)_{3-x}(OEt)_x$-HPF_6 System

KUI CHENG AND SAM ZHANG*
School of Mechanical and Aerospace Engineering, Nanyang Technological University, 50 Nanyang Avenue, 639798 Singapore
KCheng@ntu.edu.sg
MSYZhang@ntu.edu.sg.

WENGJIAN WENG
Department of Materials Science and Engineering, Zhejiang University, Hangzhou, 310027 Zhejiang, P.R. China
wengwj@zju.edu.cn.

Received February 23, 2005; Accepted October 20, 2005

Published online: 21 April 2006

Abstract. Fluoridated hydroxyapatite (FHA) has been successfully synthesized via sol-gel method with HPF_6 as the fluorine containing reagent. The chemical reactions induced by HPF_6 addition and the formation process of fluoridated hydroxyapatite (FHA) are investigated. The hydrolysis and alcoholysis of HPF_6 release F ion into the solution which, in turn, reacts with Ca ion to form nanocrystalline CaF_2 (nc-CaF_2). These nc-CaF_2 improves the gelation ability of the system through formation of F–H hydrogen bonding between F in nc-CaF_2 and H in P precursors. Increasing HPF_6 leads to more nc-CaF_2 thus less $Ca(NO_3)_2$ in the dried gel, or the presence of nc-CaF_2 in the gel suppresses the formation of $Ca(NO_3)_2$. At elevated firing temperatures, the P containing groups react with each other to form condensed phosphate. These condensed calcium phosphate, nc-CaF_2/$Ca(NO_3)_2$, reacts with the rest of the amorphous phase to form FHA phase at above 400°C.

Keywords: HPF_6, CaF_2, sol-gel processing, fluoridated hydroxyapatite, hydrogen bonding

Introduction

Bioactive coatings are usually prepared on the surface of biomedical metal implants to render good bioactivity between the host and the implant while the metallic implant provides mechanical strength for weight-bearing needs. Till now, the most prevailing bioactive coating is hydroxyapatite (HA) [1], which is proven capable of promoting implant fixation. However, in clinical application, the long term effectiveness of the HA coatings deteriorates due to relatively large dissolution of HA in body fluid [2, 3].

It is reported that fluorine incorporation into the HA structure promotes formation of fluoridated hydroxyapatite (FHA) whereby the intrinsic solubility decreases significantly while the bioactivity basically remains unchanged [4–6]. This prompts active research of FHA coatings in recent years, mostly using sol-gel method [7–9]. Results show that FHA coatings have good *in vitro* biocompatibility and bioactivity, at least comparable to pure HA.

In sol-gel method, FHA is usually synthesized by introducing fluorine containing reagent such as NH_4F, $Ca(CF_3COO)_2$, NH_4PF_6, etc. [7, 10, 11]. Successful sol-gel preparation of FHA coatings requires easy and effective way of tailoring the F concentration through chemical reactions in the reagents. These reactions will further affect the sol-gel behavior, and the gelation behavior will greatly affect the coating properties like thickness and surface morphology. In our previous work, HPF_6 was found to be effective in formation of fluoridated hydroxyapatite with controllable fluorine concentration [9, 12]. In this paper, we look into the effect of HPF_6 on sol-gel behavior during the formation of FHA and propose a formation process.

*To whom correspondence should be addressed.

Experimental

Phosphoric pentoxide (P_2O_5, GR, Aldrich) was dissolved in absolute ethanol (GR, Aldrich) to a concentration of 2 mol/L and refluxed for 24 h to be the P precursor. Calcium nitrate tetrahydrate ($Ca(NO_3)_2{\cdot}4H_2O$, GR, Aldrich) was dissolved in absolute ethanol to form 2 mol/L solutions to be the Ca precursor. Designed amounts of hexafluorophosphoric acid (HPF_6, GR, Aldrich) were added into the P precursor and then Ca precursor solution was added dropwise, adjusting the Ca/P ratio to 1.667 to be the starting solution. After further refluxing for 24 h, they turned into sols showing different state from clear to opaque depending on the initial amount of HPF_6. The exact amount of HPF_6 in each sample was listed in Table 1.

The size of particles dispersed in the opaque sol was characterized by a particle size analyzer (Malvern, Mastersizer 2000, analysis range from 20 nm to 2000 μm). Instead of standard procedure which needed the powders to be dispersed in ethanol before measurement, in this method, the sol was characterized directly. The centrifugate of the opaque sol was also characterized by XRD (Rigaku D/Max RA, 0.02° per step, 2° per minutes).

To study the reactions and phase evolution during drying and firing, the sol was dried in oven at different temperature from ambient to 250°C, and the gel resulted was further fired in furnace from 400°C to 900°C. The dried gel and fired powders were characterized by XRD (Rigaku D/Max RA, 0.02° per step, 2° per minutes) for phase identification. ^{31}P and ^{19}F liquid NMR was employed to analyze the starting solution, the refluxed sol and the fresh gel (after ultrasonically dispersing into ethanol) for their chemical state identification (BRUKER AMX300; 121.5 MHz, 85% H_3PO_4 as the reference compound for ^{31}P; 282.4 MHz, C_6F_6 as the reference compound for ^{19}F). The chemical state of P in the dried gel and fired powders were characterized by ^{31}P solid MAS NMR analysis (BRUKER MSL 400P, 161.978 MHz, 85% H_3PO_4 as the reference compound).

Results

As shown in Table 1, with increasing HPF_6 amount in the starting solution, the sol evolved gradually from clear to opaque. The isolated centrifugate was identified as CaF_2 [11]. The opaque sol ($HPF_6/Ca = 1/15$) was characterize directly for particle size (i.e. the size of CaF_2 dispersed in it). It was found that most of the particles were of about one hundred nanometers in size as shown in Fig. 1.

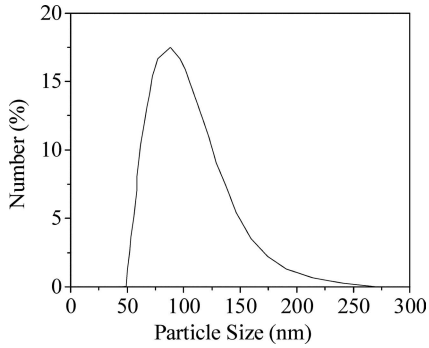

Figure 1. Particle size distribution in the sol with HPF_6/Ca ratio of 6/90.

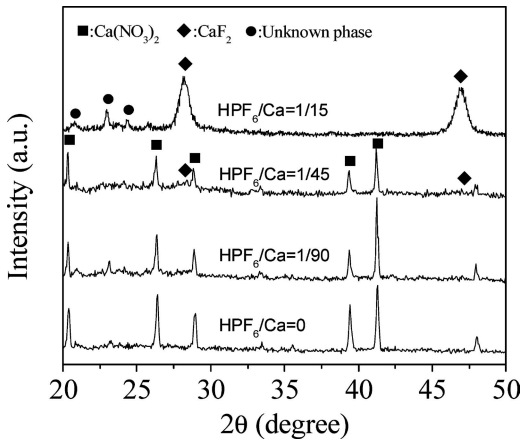

Figure 2. XRD patterns of gels for different fluorine concentration.

The gelation behavior of the sol differed greatly depending on drying temperature and evaporation. In the case of sealed container, gelation slowed down because of slower solvent evaporation. The gelation process was tabulated in Table 1. Increased HPF_6 concentration resulted in improved gelation: the higher the HPF_6 concentration, the faster the gelation. As HPF_6/Ca ratios increased from 1/30 to 1/15, the gelation time needed was reduced from 2 months to about 3 weeks. For HPF_6/Ca ratios of 0 to 1/45, no gelation occurred even after 6 months.

Figure 2 plots the XRD patterns of the FHA powders dried at 120°C for 10 h. For the sample without F or with little F (HPF_6/Ca ratio equaled to 0 and 1/90), the gel consists $Ca(NO_3)_2$ crystalline phase, amorphous phase and some unknown phases. At higher F content (HPF_6/Ca equaled to 1/45), additional weak CaF_2 peaks is observed, while the peak intensity of $Ca(NO_3)_2$ decreases. At even higher F

Table 1. Gelation behavior of the sol with different amount of HPF_6 addition (sealed, stored in ambient temperature).

HPF_6/Ca ratio	0	1/90	2/90	3/90	4/90	5/90	6/90
Mode of the sol	Clear sol	Clear sol	Light cloudy sol	Cloudy sol	Translucent sol	Nearly opaque sol	Opaque sol
After aging	Sol, 6 months	Sol, 6 months	Sol, 6 months	Gel, 2 month	Gel, 1 month	Gel, 1 month	Gel, 3 weeks

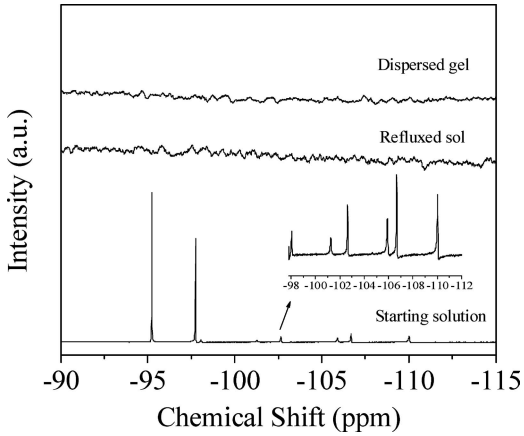

Figure 3. ^{19}F liquid NMR spectra of the starting solution, refluxed sol and fresh gel dispersed in ethanol.

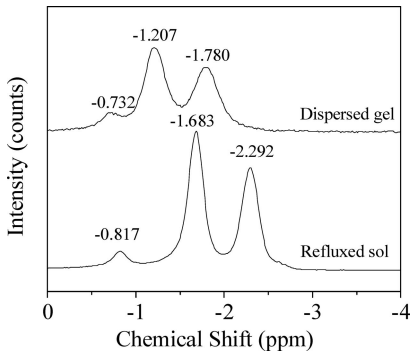

Figure 4. ^{31}P liquid NMR spectra of the refluxed sol and the fresh gel dispersed in ethanol.

content (HPF_6/Ca equaled to 1/15), crystalline CaF_2 dominates the gel phase without traces of $Ca(NO_3)_2$. The unknown phases here are regarded as transient organic crystal, since they could not be identified by existing JCPDS cards, and disappear at elevated drying temperature.

Figure 3 records ^{19}F liquid NMR spectra of the starting solution, the refluxed sol and the fresh gel dispersed in ethanol. In the starting solution, a pair of strong peaks and three pairs of weak peaks (inset) are observed. The pair of strong peaks are attributed to F in HPF_6, while the pairs of weak peaks to the transient hydrolysis and alcoholysis product of HPF_6 [11]. After refluxing or in the dispersed fresh gel, no F peaks are found (all F forms CaF_2 that precipitates).

Figure 4 plots ^{31}P liquid NMR spectra for the refluxed sol and the fresh gel. There are three peaks located at −0.817 ppm, −1.683 ppm and −2.292 ppm respectively, attributed to P in three different groups in the sol [13]: −0.817 ppm for $PO(OH)_3$, −1.683 ppm for $PO(OH)_2(OEt)$ and −2.292 ppm for $PO(OH)(OEt)_2$. The dispersed gel ^{31}P spectrum also shows three peaks: −0.732 ppm, −1.207 ppm and −1.780 ppm. The first peak experiences almost no shift, while the latter two shift to lower field significantly. These P peaks should come from those "re-dissolved" P containing

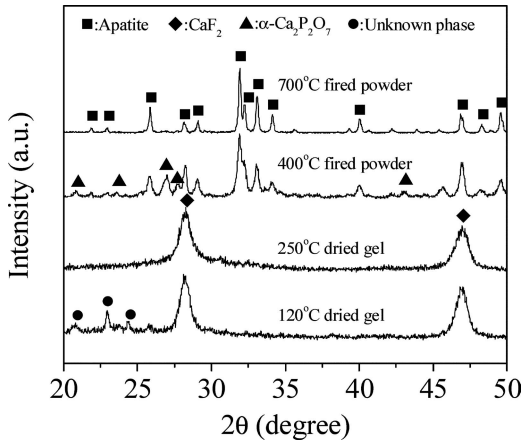

Figure 5. XRD patterns of powders and gels treated in different temperature (Derived from sols with HPF_6/Ca ratio of 6/90).

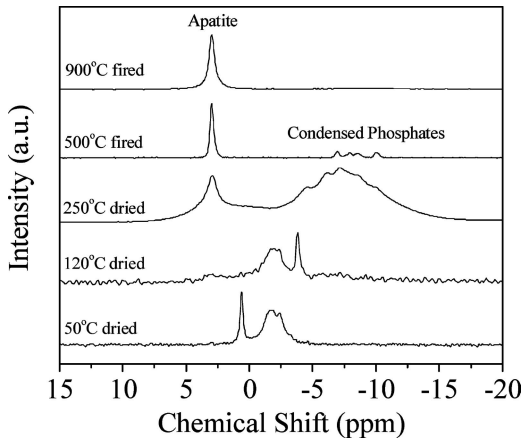

Figure 6. ^{31}P MAS NMR solid NMR spectra of powders and gels treated in different temperature (Derived from sols with HPF_6/Ca ratio of 6/90).

groups. Since the fresh gel only undergoes ambient aging (no high temperature history), no organic oxidation takes place, thus the two shifted peaks correspond to dehydrogenated form of $PO(OH)_2(OEt)$ and $PO(OH)(OEt)_2$, i.e. $[PO_3(OEt)]^{2-}$ and $[PO_2(OEt)_2]^-$ respectively.

Figure 5 plots XRD patterns of the gels dried and fired at different temperatures. Dried at 120°C, CaF_2 phase dominates with some amorphous phase and unknown phases. As the drying temperature increases to 250°C, the unknown phase disappears. As the gel is fired at 400°C, an array of phases appears: apatite, CaF_2 and α-$Ca_2P_2O_7$. At 700°C, these phases react to yield a pure apatite phase.

Figure 6 illustrates ^{31}P solid NMR spectra of powders and gel treated at different temperatures. The gel dried at 50°C exhibits a broad peak and a sharp peak. Since the temperature is not high enough to induce oxidation reaction and evaporation of H_3PO_4 [14], the sharp peak is attributed to H_3PO_4. The broader peak covering about 4 ppm appears at almost the same position to those of the $PO(OH)_2(OEt)$ and $PO(OH)(OEt)_2$, thus it is reasonable to be taken as originated from the widening and overlapping of the two

corresponding P peaks in Fig. 4. The gel dried at 120°C also exhibits two peaks where the broad peak position basically remains while a new sharp peak appears at about −4 ppm. This may result from polyphosphate induced by H_3PO_4 condensation, whose NMR peak always appears at much higher field direction than H_3PO_4 [15]. At 250°C, a peak located at about 2.972 ppm appears, signaling the P in apatite [16], plus a very broad peak at high field direction. Judging from its position and ppm coverage, this peak should have come from P in polyphosphates with different condensation degree, i.e. dimeric, trimeric, etc. At 500°C, the apatite peak becomes sharp with several small peaks at higher field positions as polyphosphates residual, which is completely gone at 900°C as only the apatite sharp peak remains at 2.972 ppm (an indication of pure apatite).

Discussion

During refluxing, HPF_6 is hydrolyzed and at the same time alcoholyzed by multi-step reaction. The F ion gradually released through hydrolysis/alcoholysis immediately reacts with Ca ion in the solution to CaF_2 [11]. The violent boiling in the solution (during the refluxing) prevents the growth and severe sedimentation of the nanocrystalline CaF_2. Thus a stable sol is resulted.

The particle size analyses show the size of the CaF_2 ranges from 50 to 250 nm, with majority at about 100 nm. However, the particle size analyzer works on particle induced laser scattering, thus only gives "how large the particles are", not necessarily "how big the crystalline grain is". XRD, however, can be of use to estimate the grain size using the Scherer's formula [17]. Using XRD pattern of HPF_6/Ca = 1/15 in Fig. 2, the calculated size of CaF_2 crystals is about 12 nanometers, about one tenth of the dispersing particle size (cf., Fig. 1). Thus under the refluxing conditions tested, growth of the CaF_2 can be only as large as about 12 nm. Agglomeration occurs to form CaF_2 particles of about 100 nm in size (and up to 250 nm). As concentration of HPF_6 in the starting solution directly affects both size and amount of CaF_2 crystals, increasing HPF_6 leads to milkier solution (Table 1) and more CaF_2 phase as is evident in the gel dried at 120°C (Fig. 2).

The solution in Fig. 3 has the most HPF_6. After refluxing, no F signal is detected. This shows that all the F ions have transferred from the liquid phase to solid phase, i.e. from HPF_6 to CaF_2. The subsequent reactions with F involved are reactions with nc-CaF_2.

Figure 2 shows that the amount of $Ca(NO_3)_2$ in the gel decreased with the increasing F-concentration. A similar trend of gelation is also tabulated in Table 1. Thus the existence and amount of nc-CaF_2 affects the gelation process. Since there are large amount of P containing groups in the sol and they do take part in the reactions, thus study of the change of the chemical environment of P will cast light on these reactions.

In the refluxed sol, P exists in three different chemical states: $PO(OH)_3$, $PO(OH)_2(OEt)$ and $PO(OH)(OEt)_2$, as shown in Fig. 4. After gelation, in Fig. 5, some changes happen to the chemical state of P in 50°C dried gel: $PO(OH)_3$ remains, while the other two states seem rather difficult to be distinguished from each other, indicating some bonding built up and that affects the chemical state of P in $PO(OH)_2(OEt)$ and $PO(OH)(OEt)_2$ groups. In view of the fact that the gelation properties improved with the existence of nc-CaF_2, it is reasonable to attribute the reactions to that between the nc-CaF_2 and P containing groups. Therefore, a hypothesis is proposed: owing to the strong electronegativity of fluorine, bonding easily forms between F in nc-CaF_2 and H in P containing groups during aging. Figure 7 illustrates this reaction. Since $PO(OH)_2(OEt)$ group has two H atoms, it can bond to two independent nc-CaF_2 particles, effectively acting to "bridge" the formation of gel networks (as shown in Fig. 7 as solid dots connecting two nc-CaF_2 particles). As a result, the gelation behavior is improved by the increasing nc-CaF_2.

In Fig. 4, the ^{31}P liquid NMR results of the dispersed gel show the existence of $[POO_2(OEt)]^{2-}$ and $[POO(OEt)_2]^{-}$ groups. That implies the H in $PO(OH)_2(OEt)$ and $PO(OH)(OEt)_2$ groups bond to other groups strongly, leading to the O–H bond broken upon ultrasonic dispersion. This further supports the hypothesis that H from the P-containing groups bonds with F from the nanocrystalline CaF_2.

Now consider the formation of hydroxyapatite: in the case of no addition of HPF_6, most Ca^{2+} ions in the gel coordinate to phosphate groups while others remain "free" to crystallize into $Ca(NO_3)_2$. These $Ca(NO_3)_2$ further react with P-groups to form hydroxyapatite. In this case, the observed apatite formation temperature is around 500°C [13] even though the decomposition temperature of pure $Ca(NO_3)_2$ is 561°C [14]. In the case of HPF_6 addition, the formation of nc-CaF_2 consumes Ca^{2+} ions, thus reducing or totally deprived the amount of crystalline $Ca(NO_3)_2$ in the gel. This facilitates formation of apatite due both to the high reactivity of nanoscale CaF_2 and the reduction or even total absence of $Ca(NO_3)_2$. As a result, pure fluorapatite

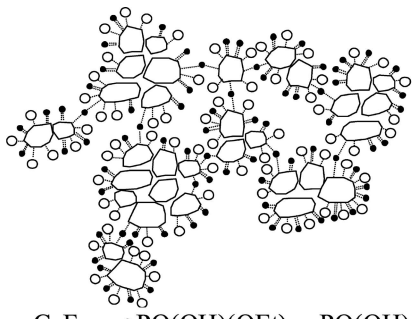

Figure 7. Schematic of gel formation through bonding of F in nc-CaF_2 and H in P-containing groups.

($Ca_{10}(PO_4)_6F_2$) appears at much lower temperature of 400°C (in Fig. 4) in the system contains HPF_6.

The temperature effect can be discerned in Figs. 5 and 6. In Fig. 5, pyrophosphate (α-$Ca_2P_2O_7$) appears at 400°C and then disappears together with CaF_2 phase at 700°C to be pure fluorapatite. That indicates a series of reactions occur before the final formation of apatite. These reactions can be seen from Fig. 6: the fact that the broad peak at about −2 ppm shows almost no change from 50°C to 120°C indicates that the chemical environment of the P in $PO(OH)_2(OEt)$ and $PO(OH)(OEt)_2$ remain unchanged; however, the disappearance of H_3PO_4 and the appearance of polyphosphate indicate all the phosphoric acid has been reacted into condensed form due to the elevated drying temperature. At even higher temperature (250°C), polyphosphate of different condensation degree is formed (as seen from the broad peak at round −7 ppm), while $PO(OH)_2(OEt)$ and $PO(OH)(OEt)_2$ groups disappear. That means these P groups have also transformed into certain kind of polyphosphate. At this temperature, there is also a peak correspondent to apatite appears (at around 2.972 ppm), it may be caused by the local overheating during drying, and the amount is too little to be detected by XRD (Fig. 5). At 400°C, formation of apatite is abundant (Fig. 5), and at the same time, formation of crystalline pyrophosphate (dimeric polyphosphate) is observed (solid triangles). At 500°C and above (Figs. 5 and 6), the remaining CaF_2 further react with α-$Ca_2P_2O_7$ to form pure apatite. In summary, the P containing groups first transform into polyphosphate (with different degree of condensation), then they react with nc-CaF_2 and turn into apatite at above 400°C. That is the case for high content of HPF_6 (thus pure fluorapatite is formed as a result). For systems of other F content, $Ca(NO_3)_2$ should still exist in different degree and in the end, CaF_2, $Ca(NO_3)_2$ and α-$Ca_2P_2O_7$ react to form FHA instead of pure fluorapatite.

Conclusion

FHA has been successfully synthesized with HPF_6 as the fluorine containing reagent. The reactions are characterized as follows:

The HPF_6 added in the starting solution hydrolyzes and alcoholyzes so that all the F transfer into CaF_2 phase during refluxing. The CaF_2 phase formed is nanocrystalline and agglomerate into clusters. The size of the crystalline CaF_2 is around 12 nm and the cluster size is 100 nm in the system where the HPF_6/Ca ratio is 1/15.

The presence of nc-CaF_2 promotes gelation of the sols by forming hydrogen bond between F in nc-CaF_2 and H in $PO(OH)_{3-x}(OEt)_x$ ($x = 1, 2$).

The gel turns into FHA when fired to above 500°C. The process can be viewed as a two-step reaction: first, P-containing groups react with each other to form polyphosphate with different degree of condensation; and then, depending on F content, these polyphosphate phases further react with nc-CaF_2 and/or $Ca(NO_3)_2$ phase to form fluoridated hydroxyapatite.

Acknowledgment

The author would like to thank the Agency for Science Technology and Research, Singapore (A∗Star project 032 101 0005) for the financial support.

References

1. K. de Groot, R. Geesink, C.P.A.T. Klein, and P. Serekian, J. Biomed. Mater. Res. **21**, 1375 (1987).
2. S. Overgaard, M. Lind, K. Josephsen, A. B. Maunsbach, C. Bnger, and K. Soballe, J. Biomed. Mater. Res. **39**, 141 (1998).
3. L. Gineste, M. Gineste, X. Ranz, A. Ellefterion, A. Guilhem, N. Rouquet, and P. Frayssinet, J. Biomed. Mater. Res. **48**, 224 (1999).
4. F.C.M. Driessens, Nature **243**, 420 (1973).
5. W.J.A. Dhert, C.P.A.T. Klein, J.A. Jansen, E.A. van der Velde, R.C. Vriesde, P.M. Rozing, and K. de Groot, J. Biomed. Mater. Res. **27**(1), 127 (1993).
6. J.E.G. Hulshoff, K. von Dijk, J.P.C.M. van. Der. Waerden, W. Kalk, and J. A. Jansen, J. Mater. Sci.: Materials in Medicine **7**, 603 (1996).
7. H. Kim, Y. Kong, and J. C. Knowles, Biomaterials **25**, 3351 (2004).
8. M. Cavalli, G. Gnappi, A. Montener, C. Bersani, P. P. Lottici, S. Karciulis, G. Mattogno, and M. Fini, J. Mater. Sci. **36**, 3253 (2001).
9. K. Cheng, W. Weng, H. Qu, P. Du, G. Shen, G. Han, J. Yang, and J. M. F. Ferreira, J. Biomed. Mater. Res. Part B, Appl. Biomater. **69B**, 33 (2004).
10. U. Partenfelder, A. Engela, and C. Russel, J. Mater. Sci. **4**, 292 (1993).
11. K. Cheng, G. Han, W. Weng, H. Qu, P. Du, G. Shen, J. Yang, and J.M.F. Ferreira, Mater. Res. Bull. **38**, 89 (2003).
12. K. Cheng, S. Zhang, and W. Weng, Surface and Coatings Technology **198,** 237 (2005).
13. W. Weng and J. L. Baptista, Biomaterials **19**, 125 (1998).
14. D. R. Lide, *Handbook of Chemistry and Physics*, 85th edition, (CRC Press, Boca Raton, 2004), p. 4–49.
15. J. Livage, P. Barboux, M. T. Vanderborre, C. Schmutz, and F. Taulelle, J. Non-Cryst. Solids **147&148**, 18 (1992).
16. J.P. Cassella, P.J. Barrie, N. Garrington, and S. Y. Ali, J. Bone and Mineral Metabolism **18**, 291 (2000).
17. G. Jiang and D. Shi, J. Biomed. Mater. Res. **48**, 117 (1999).